An Optical Scattering Based Cost-Effective Approach Towards Quantitative Assessment Of Turbidity And Particle Size Estimation In Drinking Water Using Image Analysis

Soumendra Singh [1], Animesh Halder [1,2], Amrita Banerjee [1], Md. Nur Hasan[3], Arpan Bera[3], Oindrila Sinha[4], Sanjay K. Ghosh[5], Amitabha Mitra[5] and Samir Kumar Pal [1,3 *]

[1]*Technical Research Centre, S. N. Bose National Centre for Basic Sciences, Block JD, Sector-III, Salt Lake, Kolkata:700 106, India*

[2]*University of Calcutta, Department of Applied Optics and Photonics, JD-2, Sector-III, Salt Lake, Kolkata: 700 106, India*

[3]*Department of Chemical, Biological and Macromolecular Sciences, S. N. Bose National Centre for Basic Sciences, Block JD, Sector-III, Salt Lake, Kolkata:700 106, India*

[4]*Department of Life Sciences, Presidency University, 86/1, College Street road, Calcutta University, Kolkata 700073*

[5]*Center for Astroparticle Physics and Space Science, Bose Institute, Sector-III, Salt Lake, Kolkata: 700091, India,*

*Samir Kumar Pal, Email: skpal@bose.res.in

ABSTRACT

Contaminated water consumption primarily for drinking purposes is the cause of approximately 502,000 global deaths every year mostly in economically challenging countries indicating the need for a cheap, easy to use a yet robust and scientifically proven method for determination of water quality. In this work, we have characterized the water quality utilizing the principles of optical scattering by the suspended particulate matter using a low-cost wireless-enabled camera. The images grabbed by the camera on an optically lit cast screen on a red and a blue dot were allowed to arrive through a “model scattering medium". An estimate of the amount of light reaching the detector camera essentially provide Optical Density of the medium. Edge blurring of the captured images reveals information of the suspended particulates (sizes) in the medium. The individual pixel information was analyzed and the 'edge blurring' phenomenon was shown on an RGB intensity curve. The average diameter of the dominant suspended particles presents in the model scattering medium is also estimated from the fitting parameters and compared with that from commercially available Dynamic Light Scattering (DLS) instrument. The system is effective in measuring bacterial growth and the acquired data have been compared with that of the growth curve obtained from the gold standard method. Limit of Detection (LOD) of the set-up was found to be 48 ppm. The extremely cost-effective nature of the set-up, the innovative method of analysis, and easy availability of components would expectedly make water quality assessment very easy and user friendly.

1. INTRODUCTION

Increasing environmental pollution is a matter of grave concern in modern society(Wang, Webber, Finlayson, & Barnett, 2008). Pollution extends from air, sound, and water (Burningham & Thrush, 2004; Gorman, 2001). Among these, water pollution has shown a significant increase with the growing population index particularly in Low and Middle-Income Countries (LMIC) (Suk et al., 2016; Thomas, Wickramasinghe, Mendis, Roberts, & Foster, 2015). A worldwide minimum of 2 billion people consumes water for drinking, contaminated with fecal matter (Kimani-Murage & Ngindu, 2007). Contaminated water is the root cause of deadly diseases such as diarrhea, cholera, dysentery as well as typhoid, and its consumption results in 502,000 diarrheal deaths annually (Dwight, Fernandez, Baker, Semenza, & Olson,

2005; Kimani-Murage & Ngindu, 2007). These data indicate the urgent need for quantitative assessment of water quality including lakes(Li et al., 2007) and bigger water bodies with online determination of results indicating the readiness of consumption of available drinking water. Water quality is determined by its chemical, physical, and biological content (Lawson, 2011; Ramalho, Cunha, Teixeira, & Gibbs, 2001; Sadeghi, Mohammadian, Nourani, Peyda, & Eslami, 2007). The assessment is mainly a manual process and conventionally it is done by the collection of water samples and using chemical and other methods of analysis (Farré & Barceló, 2003). The processes are complex, suitable only for a trained person (Tebbutt, 1997). Moreover, they are time-consuming and offline (Lenat, 1988). With the advent and development of sensor-based systems, substantial research has been carried out to automate and real-time monitor the water quality and Internet of Things (IoT) enable devices are in demand for immediate intimation of human action needed anywhere (O'Flynn et al., 2007). Such sensor-based systems mainly focus on the total dissolved solvents (TDS) and pH properties of water and few such sensors have been made commercially available also. While online sensors ensure immediate data availability and trigger the need for urgent action, their calibration, reliability, and water-induced stains become an important concern (Lambrou, Anastasiou, Panayiotou, & Polycarpou, 2014). Some alternate experimental methods were also tried by researchers like using the bioscreen microbiological growth analyser (Johnston, 1998) and underwater imaging systems(Ouyang et al., 2013; Selmo et al., 2017).

Various methods of probing water quality have been tried and researched by various scientists (Association & Association, 1989). The contemporary research in this direction includes the measurement of ocean watercolor and estimation of its effect on marine biology (Barale, 1991; Shujing & Zhihua, 2001). RGB analysis has been used to determine the salinity index of water by using the ration of R to B and B to G was used to determine the chlorophyll content of water (Goddijn & White, 2006). Airborne digital image photography has also been

used to map water pollution and overcome the problem of cloud cover scenes (Kallio et al., 2001). Recently, computer vision and artificial intelligence have witnessed their application in the measurement of water turbidity and related parameters (Zion, 2012). Various methods of estimation of coliforms in drinking water have been tried as a measure to estimate water quality(Rompré, Servais, Baudart, De-Roubin, & Laurent, 2002). In our present study, we have used image analysis of a Red and a Blue dots on an optically lit cast screen across a model turbid medium to estimate the optical density (turbidity) and computational analysis of the captured image-edge blurring phenomena to conclude on the diameter of dominant suspended particulate matter in the turbid colloidal solution. We have also explored the possibility of using a submersible camera to acquire data for long term data acquisition of a natural water body. Data acquired remotely has been analyzed in our indigenously developed software for online monitoring. The proposed set-up finally produces real-time data of particle size estimation and fitness of consumption of contaminated water samples with sub-micron suspended particulate matter, which are difficult to assess via visual inspection. The developed set-up efficiently estimates the presence of suspended particulate matter including micro-organism to a level of 48 ppm (and hence defines the LOD of the system) which is well below the WHO level of 300 ppm in drinking water (Organization, 2003). Water samples with coarser particles will be easier to identify and screen for consumption visually have not been included in this study.

2. MATERIALS AND METHODS

2.1. Cast Screen

An optically backlit cast screen was used to draw the Red and Blue dots. The 220 VAC LED lamp was purchased from Philips and was fitted with an optical diffuser to block the direct beam saturating the receiver (camera). The dots of 1 cm diameter were printed from a calibrated true color printer (HP 2280). The wavelengths corresponding to individual colors were determined from the reverse calculation of RGB value with wavelength correlation. The

submersible camera (QAWACHH) was purchased online. “Y-camera” app was used to acquire live images on a laptop or smartphone. Quartz cuvette was held in between as a sample holder ensuring a clear field of view of the cast screen through the sample.

2.2. Preparation of Samples

The same quality milk samples were prepared at various concentrations starting from 1μL to 40 μL in 1 mL of whole raw milk. The purchased sample was maintained at the highest purity level to the best of knowledge. The standard pipetting apparatus (Accupipet) was used to extract the exact amount of solution under test.

2.3. Camera Characterization

Computer vision mainly suffers from the problem of auto-brightness and auto saturation of pixels (Hu, Gallo, Pulli, & Sun, 2013). This leads to unequal referencing of data under various ambient light conditions. However, the choice of camera was made to be able to manually adjust the focus and exposure. Moreover, important considerations were taken to ensure submerged condition water protection for electronics and camera optics. To tackle this problem, a mobile endoscope camera enabled with in-built wireless LAN was used to capture images and transfer to a distant computer or mobile in real-time.

2.4. Development of low-cost instrument and Its Working Principle

The working principle of this device is primarily based on the scattering and absorption of light by suspended particulate matters in a colloidal solution. Fig. 1 shows the schematic diagram of the experimental arrangement. A backlit screen (diffusor) has been used as a cast screen. Two colors Red and Blue have been utilized as a marker of distinctly apart wavelength with no overlap of the spectrum. Light from the screen travels to the wireless camera after interacting with the sample in the cuvette. The camera has been strategically placed keeping in mind the view angle to cover both dots which are kept ensuring equal illumination behind both. The camera can be kept submerged under real-life situations and is enabled with wireless LAN to

ensure remote monitoring of the sample. Light traveling from the screen will suffer absorption by the sample guided by Beer-Lambert's law. However, light traveling at the edge of the sample will suffer multiple reflections and will result in blurring of the edges as depicted conceptually in Fig. 2(a). The indigenously developed machine-computer interface will acquire live images and will do a pixel analysis of the entire image frame to quickly calculate the amount of light absorbed as well as particle size estimation of the dominant component. Fig. 2(b) shows the pattern of fade experienced by the edge of the image as one moves away from the center of the circle.

2.5. Interfacing Software Design

A LabVIEW based program is designed to acquire and process data from the instrument via a USB port. A Microsoft-Windows based on-board computer is used to run the developed software in real-time to acquire data. The interface is made to be simple and intuitive, thus, no requirement of any additional training to operate the software. The software identifies the attached camera and grabs video frames. It then does frame by frame pixel RGB analysis and extracts the Red and Blue information from the similar color dots respectively. The software also plots the value in real-time and tries to identify the edge and performs an online fitting of a sigmoidal function. The derived values are a marker of various parameters of the suspended particulate matter.

2.6. Bacterial Growth curve experiment

The bactericidal activity is performed using MRSA *(methicillin-resistant staphylococcus aureus)* bacteria cells. The cells are cultured in a Luria Broth (LB) medium under an incubator shaker at 37 °C for 24 h. The optical density of freshly grown overnight culture is fixed to 0.1 in LB medium initially. The culture is then put in a cuvette and incubated at 37°C with shaking for 9 h. The absorbance is taken at every hour interval and plotted against time with baseline correction. The minimum detectable concentration of MRSA was determined using the onset

of the growth curve. To estimate the limit of detection (LOD) of the suspended micro-organism (MRSA), we have converted the concentration of the micro-organism in the media from CFU/ml to ppm unit.

2.7. Crystal Violet (CV) Staining Assay

The freshly diluted culture of MRSA is spread over a biofilm and kept in an incubator at 37°C for 24 h. Then, 1% of CV solution is spread over biofilm and incubated for 3 h. After washing with water, the biofilm is exposed under a microscope (Leica digital inverted microscopes DMI8).

3. RESULT AND DISCUSSION

The acquired video is analyzed frame by frame. Individual frames were performed a raster scan for pixel RGB information. Fig. 3(a) shows the intensity plot of Red value (from RGB analysis) obtained from Red-colored dot. Similar results were obtained from the blue dot after extraction of blue value (from the RGB analysis) as evident from Fig. 3(b). The curves were fitted with a sigmoidal function. The fitting parameters obtained were found to be markers of absorption and scattering parameters of the sample under test. The fitted equation was,

$$\boldsymbol{y = A_2 + \frac{(A_1 - A_2)}{\left(1 + e^{\left((x-x_0)/dx\right)}\right)}} \qquad \text{(i)}$$

The value of X_0 obtained from the fitting function from individual curves is plotted against concentration for light red n blue dots as shown in Fig. 4(a & b) respectively. The parameter is found to be indicative of the broadening of the edges due to Rayleigh scattering of optical signals by the suspended particulate matter. The pixel profile plot is expected to show a shift of intensities towards the negative X-axis to represent the broadening to the colored dot on the left edge. This was confirmed by plotting X_0 profile with concentration as shown in Fig. 3 (a & b). The curve clearly shows the linearly decreasing profile with increasing concentration suggesting a significant broadening of edges which is a signature of number and size

distribution of colloidal substance present in an optically turbid solution. Hence, the broadening of edges becomes the signature of the number of scattering materials present in the colloidal suspension.

The diameter of particles in colloidal suspension can be estimated from the following well known Rayleigh scattering equation (ii). The intensity I of light scattered by anyone of the small spheres of diameter d and refractive index n from a beam of unpolarized light of wavelength λ and intensity I_0 is given by

$$\boldsymbol{I = I_0 \frac{1+\cos^2\theta}{2R^2}\left(\frac{2\pi}{\lambda}\right)^4\left(\frac{n^2-1}{n^2+1}\right)^2\left(\frac{d}{2}\right)^6} \quad \text{(ii)}$$

where R is the distance to the particle and θ is the scattering angle.

Our experimental set-up dictates the use of two distinct wavelengths which was derived by conversion of RGB parameters to respective colors and further to specific wavelengths. The derived wavelengths were found to be $\lambda = 700$ nm for red color and $\lambda = 450$ nm for blue color.

The above equation (ii) can be re-written as the following:

$$\boldsymbol{d^6 = \frac{1}{(1+\cos^2\theta)\left(\frac{m^2-1}{m^2+2}\right)^2}\frac{8R^2\lambda^4}{\pi^4}\frac{I}{I_0}} \quad \text{(iii)}$$

Therefore,

$$\boldsymbol{d^6 = K\,\frac{I}{I_0}} \quad \text{(iv)}$$

Where K is the constant and is governed by the equation

$$\boldsymbol{K = \frac{1}{(1+\cos^2\theta)\left(\frac{m^2-1}{m^2+2}\right)^2}\frac{8R^2\lambda^4}{\pi^4}} \quad \text{(v)}$$

After calculation using the above-mentioned values of parameters we get,

$K=2.589 \times 10^{-30}$ for blue (considering $\lambda_{Blue}= 450$nm, R=4mm and $(1+\cos^2\theta) =1.99952$) and

$K = 1.516 \times 10^{-29}$ for red (considering $\lambda_{Red}= 700$nm, R=4mm and $(1+\cos^2\theta) =1.99956$)

$$\mathbf{6 \log d = \log k + \log \frac{I}{I_0}} \quad \text{(vi)}$$

$$\mathbf{6 \log d = \log k - \log \frac{I_0}{I}} \quad \text{(vii)}$$

The term $\log \frac{I_0}{I}$ is the signature of Beer Lambert's law which is synonymous to the parameter A2-A1 of our fitting function. From equation (vii) we have calculated out for 450 nm wavelength as 252 nm and for 700 nm wavelength to be 730 nm which is in very close approximation with the standard DLS data as shown in Fig. 5. indicating the variation of the diameter size of the dominant scatterer present in the sample with increasing concentration. It was found that the diameter estimated using our set-up was in close agreement with the results from the DLS using the gold standard instrument.

The fitting parameter (A_2-A_1) represents the extinction coefficient of the light. The amount of light traveling from the screen to the camera suffers absorption and scattering from the sample media. The difference of pixel information from normal spots to colored dotted spots represents the amount of light lost during forwarding travel towards the camera. The two dots represent two dominant wavelengths and carry spectroscopic information relating to the colloidal sample. (A_2-A_1) is an indicative parameter towards the Optical Density of the sample governed by Beer lambert's law as shown in Fig. 6 (a & b). The choice of milk as a simulation of turbid water samples was found to be appropriate as we found a substantial similarity between particle size estimation from DLS instrument using the refractive index of various particles found in real-world water samples e.g. silica with the same. Fig. 7 shows the comparison of number concentration data obtained via DLS instrument using the refractive index of silica and milk respectively. Using our set-up, the effective diameters were found to be 6.8 μm using blue dot whereas using the red dot we arrived at the diameter of 10.9. Once again better approximation was observed using blue dot depicting the effectiveness of the set-up in a lower range of visible wavelengths.

Fig. 8 attributes the standardized growth curve of MRSA. Herein, after the short (of 1h) lag phase, optical density is exponentially increased up to 8 h (log phase). The measurement of population growth is also manifested by image processing of red and blue dots. It is found that the growth curve exhibited by the blue dot showed much higher sensitivity and quick response to the growth of MRSA. However, it also exhibits quick saturation commensurate with a standardized growth curve. In contrast, the response obtained from the Red curve is found to be less responsive compared to the standard growth curve but showed no signs of saturation with increasing time. It can be concluded that from this strategy, we can get two sensing curves, one will better sensitivity as well as a response but the lower dynamic range and the other with a lesser response but with a wider dynamic range. The bacterial growth curve was acquired using blue and red dot images. The minimum detectable concentration from the blue curve was found to be 48 ppm and the corresponding red curve was found to be 448 ppm. The LOD for the gold standard method was found to be 52 ppm.

The average hydrodynamic diameter of MRSA is found to be 1µm from DLS as evident from Fig 9 (a). As shown in Fg 9 (b) the microscopic image of MRSA designates the cell diameter is approximately 0.8µm which is in good agreement to our findings 5.6 µm from our developed technique. It is to be noted the values are sometimes over-estimated due to the accumulation of multiple molecules as shown in Fig 9 (b).

4. CONCLUSIONS

In this work, we have presented a simple, innovative, and cost-effective technique involving the analysis of a video captured from a camera and estimate the amount of turbidity and also suspended particle size. The data have been analyzed using an indigenously developed software for online analysis of the model turbid medium. The set-up is found to be effective in calculating the above-mentioned parameters quickly and with a fair amount of accuracy. We also have investigated the possibility of assessment of bacterial presence in water with a fair

amount of accuracy. We hope the developed strategy with quick, easy, and precise determination of water quality with reasonably low LOD of suspended particulate matter (48 ppm) would offer an affordable alternative in a low resource setting for developing countries. The technology can be further applied to assess air quality and visibility assessment in a foggy atmosphere. However, more experimentation is required before the same can be established.

5. FUNDING

The study is funded by DST under the Technical Research Centre of the S. N. Bose National Institute for Basic Sciences and IRHPA (Intensification of Research in High Priority Areas/Sanction No. IR/S2/PF.01/2011) of Bose Institute.

6. CONFLICT OF INTEREST

The authors declare no conflict of interest.

7. REFERENCE:

Association, A. P. H., & Association, A. W. W. (1989). *Standard methods for the examination of water and wastewater*: American public health association.

Barale, V. (1991). Sea surface colour in the field of biological oceanography. *International Journal of Remote Sensing, 12*(4), 781-793.

Burningham, K., & Thrush, D. (2004). Pollution concerns in context: a comparison of local perceptions of the risks associated with living close to a road and a chemical factory. *Journal of Risk Research, 7*(2), 213-232.

Dwight, R. H., Fernandez, L. M., Baker, D. B., Semenza, J. C., & Olson, B. H. (2005). Estimating the economic burden from illnesses associated with recreational coastal water pollution—a case study in Orange County, California. *Journal of Environmental management, 76*(2), 95-103.

Farré, M., & Barceló, D. (2003). Toxicity testing of wastewater and sewage sludge by biosensors, bioassays and chemical analysis. *TrAC Trends in Analytical Chemistry, 22*(5), 299-310.

Goddijn, L., & White, M. (2006). Using a digital camera for water quality measurements in Galway Bay. *Estuarine, coastal and shelf science, 66*(3-4), 429-436.

Gorman, H. S. (2001). *Redefining efficiency: pollution concerns, regulatory mechanisms, and technological change in the US petroleum industry*: The University of Akron Press.

Hu, J., Gallo, O., Pulli, K., & Sun, X. (2013). *HDR deghosting: How to deal with saturation?* Paper presented at the Proceedings of the IEEE Conference on Computer Vision and Pattern Recognition.

Johnston, M. D. (1998). A simple and rapid test for quality control of liquid media, using the bioscreen microbiological growth analyser. *Journal of microbiological methods, 32*(1), 37-43.

Kallio, K., Kutser, T., Hannonen, T., Koponen, S., Pulliainen, J., Vepsäläinen, J., & Pyhälahti, T. (2001). Retrieval of water quality from airborne imaging spectrometry of various lake types in different seasons. *Science of the Total Environment, 268*(1-3), 59-77.

Kimani-Murage, E. W., & Ngindu, A. M. (2007). Quality of water the slum dwellers use: the case of a Kenyan slum. *Journal of Urban Health, 84*(6), 829-838.

303 Lambrou, T. P., Anastasiou, C. C., Panayiotou, C. G., & Polycarpou, M. M. (2014). A low-cost sensor
304 network for real-time monitoring and contamination detection in drinking water distribution
305 systems. *IEEE sensors journal, 14*(8), 2765-2772.
306 Lawson, E. (2011). Physico-chemical parameters and heavy metal contents of water from the
307 Mangrove Swamps of Lagos Lagoon, Lagos, Nigeria. *Advances in biological research, 5*(1), 8-
308 21.
309 Lenat, D. R. (1988). Water quality assessment of streams using a qualitative collection method for
310 benthic macroinvertebrates. *Journal of the North American Benthological Society, 7*(3), 222-
311 233.
312 Li, R., Dong, M., Zhao, Y., Zhang, L., Cui, Q., & He, W. (2007). Assessment of water quality and
313 identification of pollution sources of plateau lakes in Yunnan (China). *Journal of Environmental*
314 *Quality, 36*(1), 291-297.
315 O'Flynn, B., Martinez-Catala, R., Harte, S., O'Mathuna, C., Cleary, J., Slater, C., . . . Murphy, H. (2007).
316 *SmartCoast: a wireless sensor network for water quality monitoring.* Paper presented at the
317 32nd IEEE Conference on Local Computer Networks (LCN 2007).
318 Organization, W. H. (2003). Silver in drinking-water. Background document for preparation of who
319 guidelines for drinking-water quality: WHO/SDE/WSH/03.04/14. 2003. Available online:
320 http://www. who. int/entity ….
321 Ouyang, B., Dalgleish, F. R., Caimi, F. M., Giddings, T. E., Shirron, J., Vuorenkoski, A. K., . . . Nootz, G.
322 (2013). Compressive sensing underwater laser serial imaging system. *Journal of Electronic*
323 *Imaging, 22*(2), 021010.
324 Ramalho, R., Cunha, J., Teixeira, P., & Gibbs, P. A. (2001). Improved methods for the enumeration of
325 heterotrophic bacteria in bottled mineral waters. *Journal of microbiological methods, 44*(2),
326 97-103.
327 Rompré, A., Servais, P., Baudart, J., De-Roubin, M.-R., & Laurent, P. (2002). Detection and enumeration
328 of coliforms in drinking water: current methods and emerging approaches. *Journal of*
329 *microbiological methods, 49*(1), 31-54.
330 Sadeghi, G., Mohammadian, M., Nourani, M., Peyda, M., & Eslami, A. (2007). Microbiological quality
331 assessment of rural drinking water supplies in Iran. *Journal of agriculture & social sciences,*
332 *3*(1), 31-33.
333 Selmo, D., Sturt, F., Miles, J., Basford, P., Malzbender, T., Martinez, K., . . . Bevan, G. (2017).
334 Underwater reflectance transformation imaging: a technology for in situ underwater cultural
335 heritage object-level recording. *Journal of Electronic Imaging, 26*(1), 011029.
336 Shujing, P. D. L. S. L., & Zhihua, M. (2001). The Application of Watercolor Remote Sensing in
337 GeneralManagement of Coast Zone [J]. *Spacecraft Recoery & Remote Sensing, 2*.
338 Suk, W. A., Ahanchian, H., Asante, K. A., Carpenter, D. O., Diaz-Barriga, F., Ha, E.-H., . . . da Silva, E. R.
339 (2016). Environmental pollution: an under-recognized threat to children's health, especially in
340 low-and middle-income countries. *Environmental health perspectives, 124*(3), A41-A45.
341 Tebbutt, T. H. Y. (1997). *Principles of water quality control*: Elsevier.
342 Thomas, E., Wickramasinghe, K., Mendis, S., Roberts, N., & Foster, C. (2015). Improved stove
343 interventions to reduce household air pollution in low and middle income countries: a
344 descriptive systematic review. *BMC public health, 15*(1), 650.
345 Wang, M., Webber, M., Finlayson, B., & Barnett, J. (2008). Rural industries and water pollution in
346 China. *Journal of Environmental management, 86*(4), 648-659.
347 Zion, B. (2012). The use of computer vision technologies in aquaculture–a review. *Computers and*
348 *electronics in agriculture, 88*, 125-132.
349
350
351
352

FIGURES AND TABLES

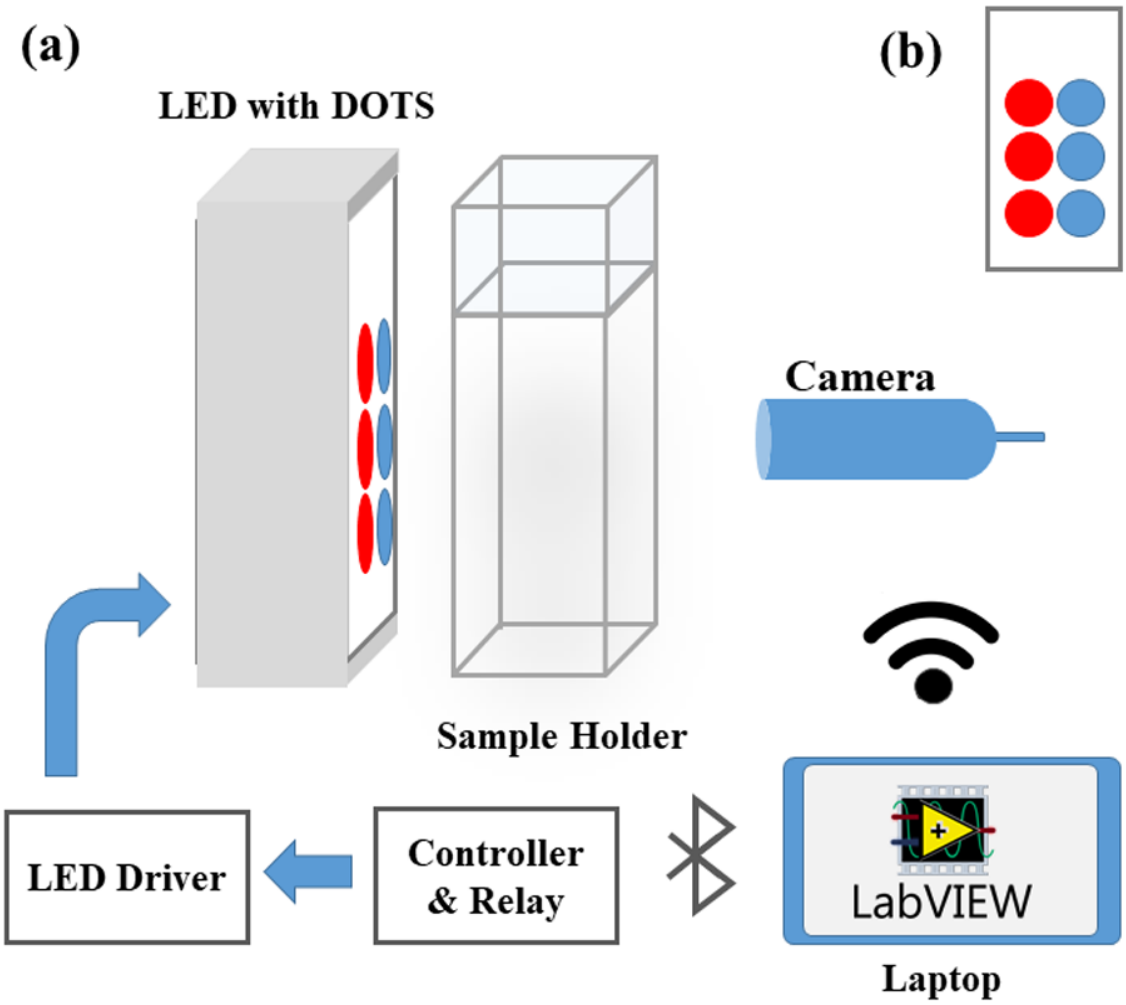

Fig*ure*. 1: (a) Schematic of the experimental arrangement for measuring optical signals from backlit cast screen (b) The dots of particular color representing the various segments of visible spectra

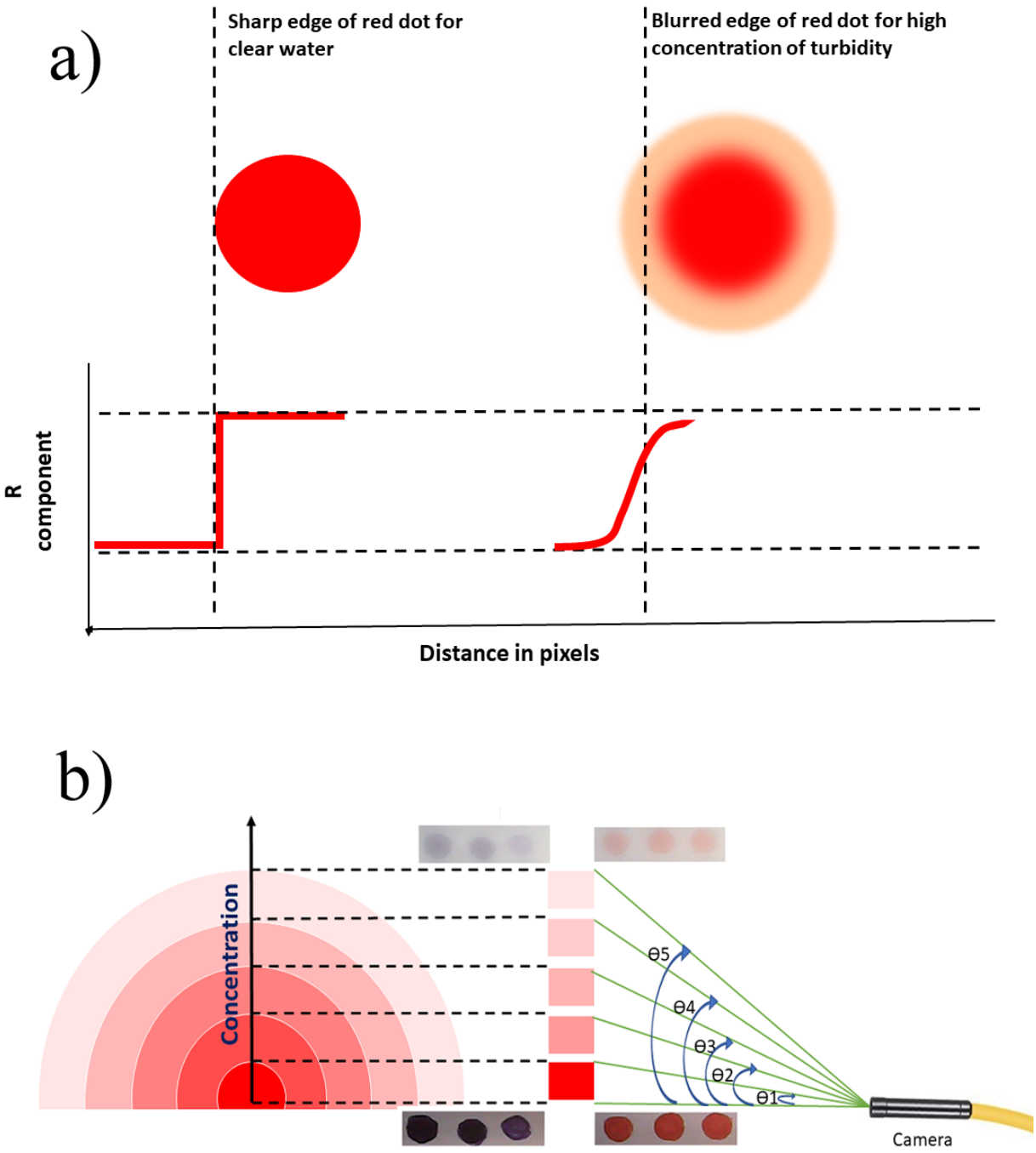

Figure. 2: a) Schematic of the image analysis method. Clearwater image of a dot as seen by a camera. The pixel intensity plot relative to the pixel position gives a sharp rising edge of a pulse function. Pixel intensity plot of turbid water and schematic of turbid water image b) Schematic of the relationship of blurring the edge of acquired images in turbid water

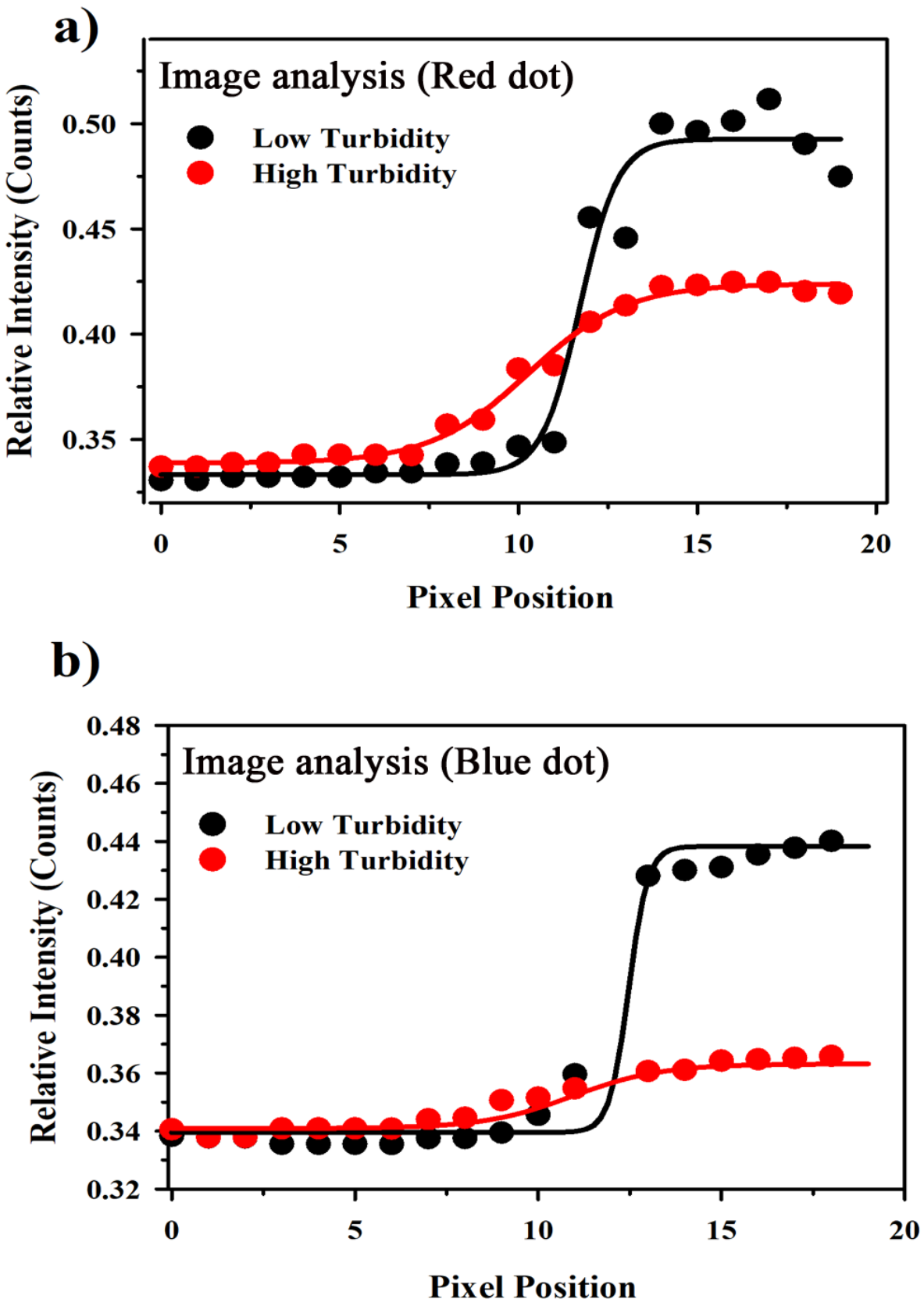

Figure. 3: a) Pixel intensity plot of acquired images of the Red dot in clear and turbid water and their respective Boltzman fitting (b) Pixel intensity plot of acquired images of the Blue dot in clear and turbid water and their respective Boltzman fittings (solid lines)

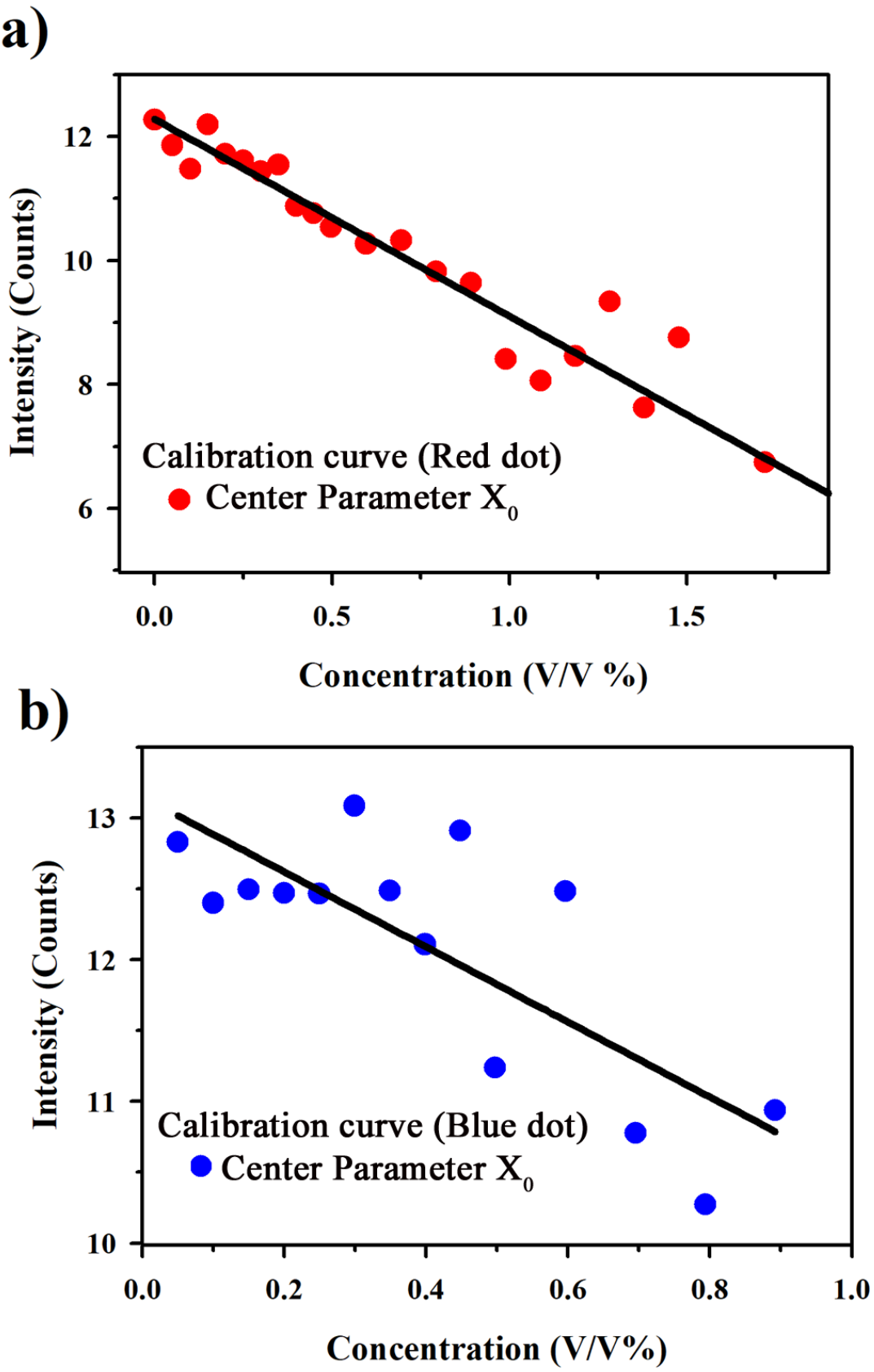

Figure 4: a) Plot of fitted center parameter X_0 with concentration for red dot b) Plot of fitted center parameter X_0 with concentration for the blue dot

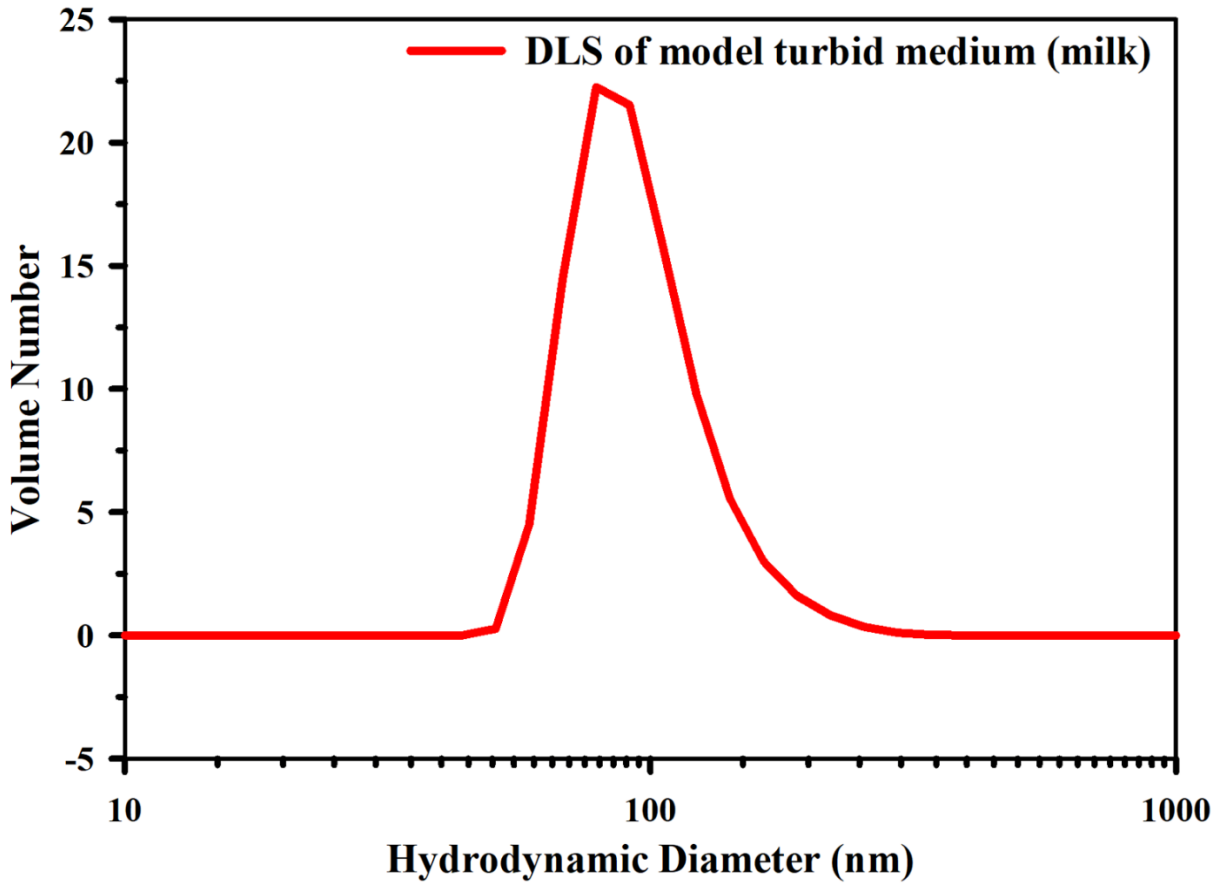

375
376 Figure. 5: DLS data of the fitting function of a sample colloidal solution (Milk)

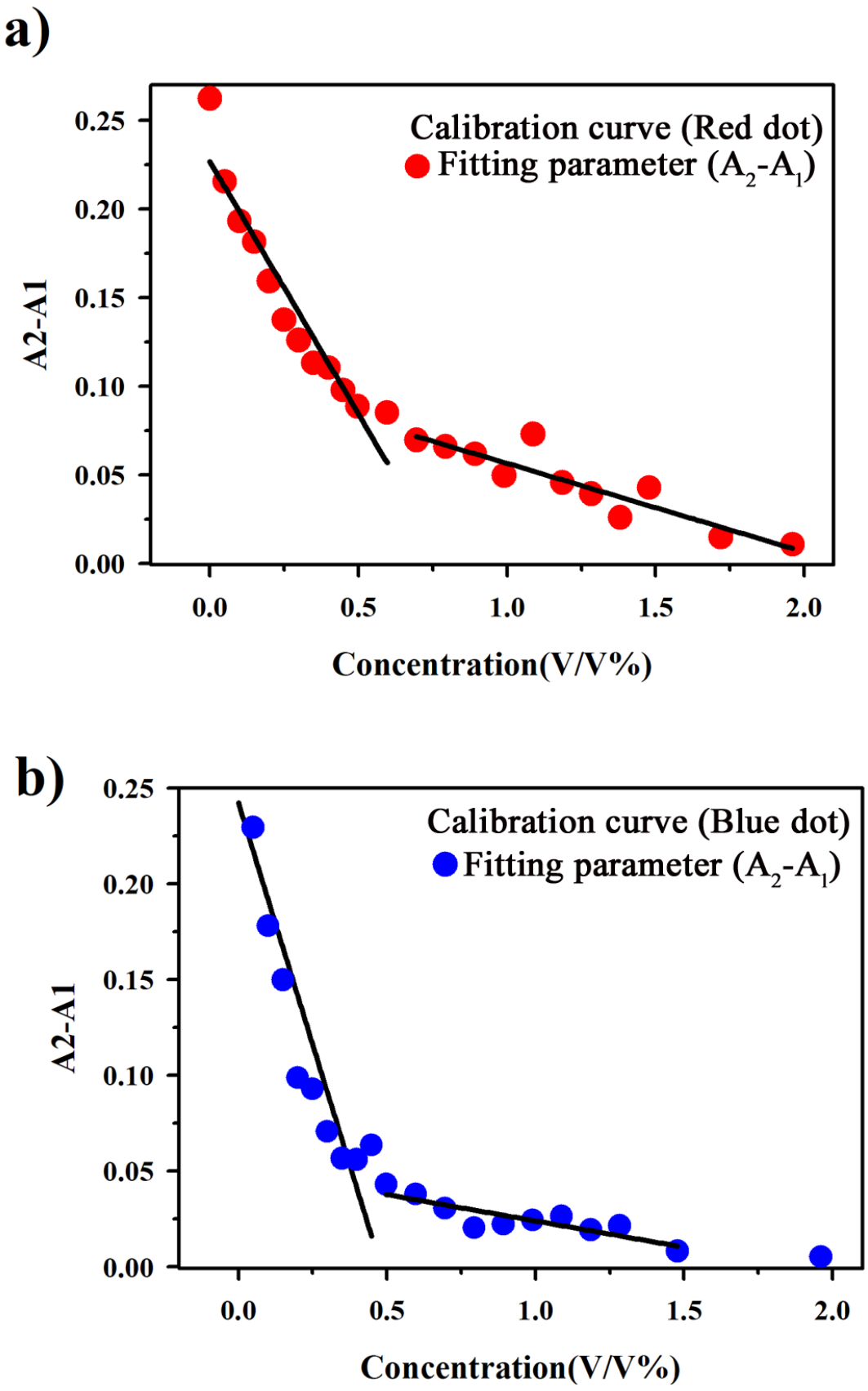

Figure. 6:. a): Plot of the fitted parameter indicating a difference of initial and final amplitudes (A_2-A_1) and its dual linear fitting function for red dot (b) Plot of the fitted parameter indicating a difference of initial and final amplitudes (A_2-A_1) and its dual linear fitting function for the blue dot.

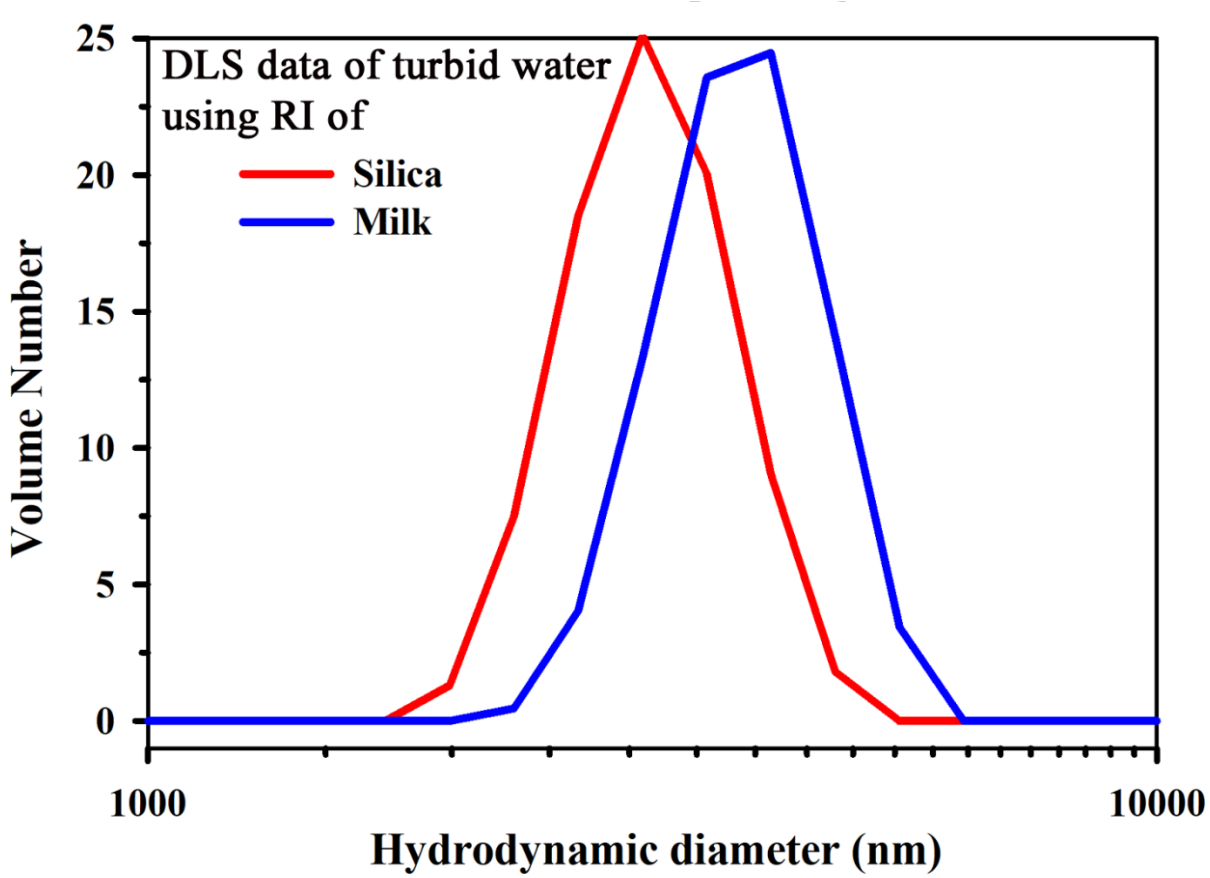

Figure. 5: Particle size distribution of turbid water samples collected locally and measured with DLS using refractive index (RI) of silica and milk respectively.

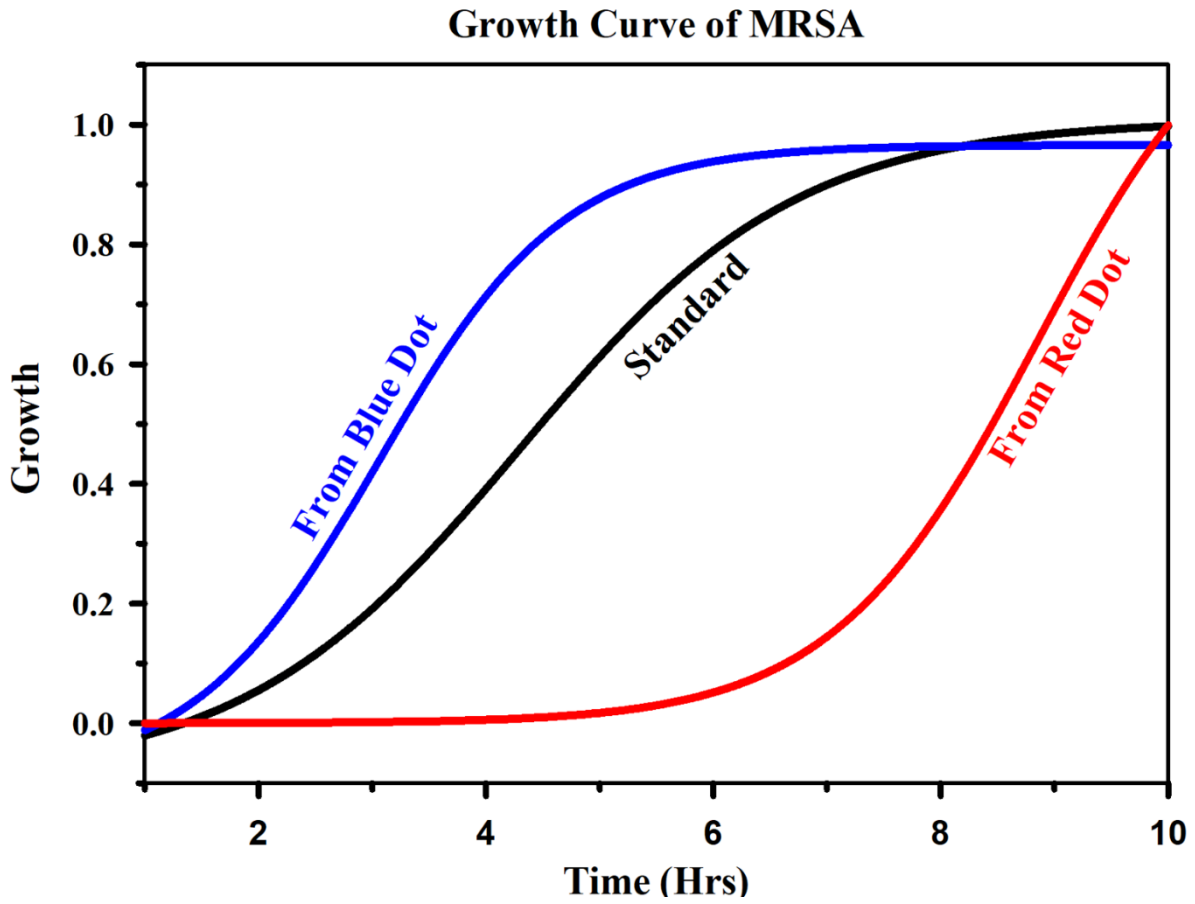

Figure. 6: Growth curve as obtained from the standard process in comparison to the developed strategy.

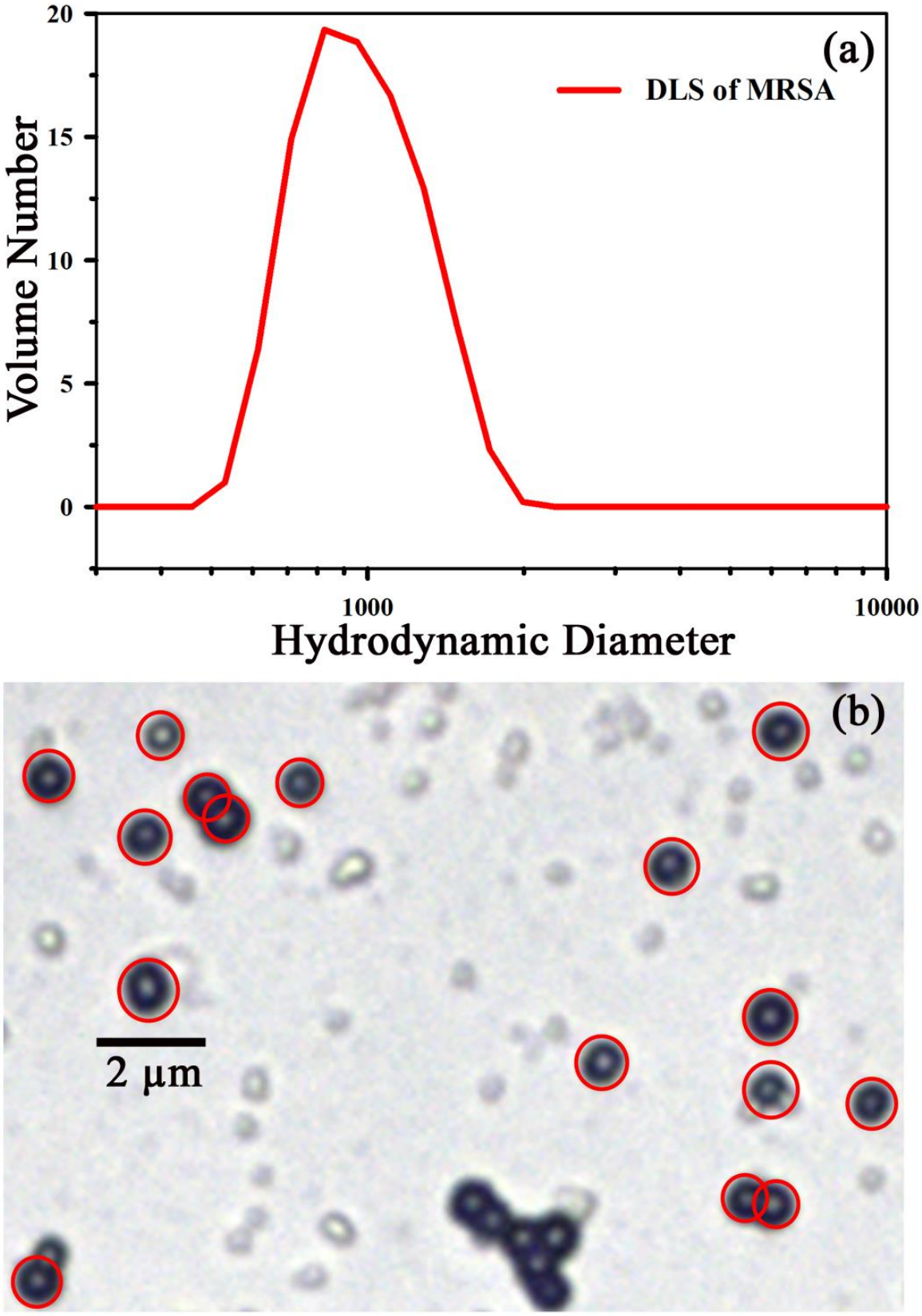

Figure. 7: (a) DLS data of MRSA exhibiting hydrodynamic diameter around 1 micron. (b) Microscopic image of MRSA confirming the diameter of around 1 micron..